

COMPUTATIONAL SIMULATION OF LARGE DROPLET ICING

William B. Wright
NYMA, Inc.
Brook Park, OH

Mark G. Potapczuk
NASA Lewis Research Center
Cleveland, OH

Abstract

Certification for flight into known icing remains one of the more challenging goals for aircraft manufacturers. This activity has been further complicated by the current interest in large droplet icing. Due to the lack of data available on the meteorology of this phenomena, there is currently an incomplete picture of the nature of the condition and even less information on its impact on aerodynamic performance. This paper describes current simulation tools available at NASA Lewis Research Center, their capabilities, and future development goals with respect to large droplet icing simulation.

Introduction

Computational simulation of the ice accretion process and its effects on aircraft performance has been undertaken by various researchers¹⁻⁸ in recent years. Results have indicated that simulation of rime ice accretions, for the range of icing conditions required for compliance with FAR 25 guidelines, can be done with a high degree of confidence in the accurate reproduction of experimentally produced ice shapes, whether they were produced in-flight or in a ground based facility. On the other hand, the accurate reproduction of glaze ice accretions remains an elusive goal due to

the complexity of the process and the lack of a complete understanding of some of the underlying physics. In the area of computational simulation of aerodynamics associated with iced airfoil geometries, there is a similar degree of fidelity available from current methods. Previous researchers⁶⁻⁸ have shown that the current computational methods can provide information on integrated parameters such as lift and drag but a complete reproduction of the details surrounding the boundary layer characteristics on the rough ice surface has yet to be completed.

Currently, there is a desire to be able to extend the use of these simulation methods to include the so-called large droplet regime (i.e. 40 μm to 400 μm diameters). In this paper we will indicate the current capability available for computational simulation of large droplet icing conditions by presenting results from the NASA ice accretion code LEWICE and a NASA Naviér-Stokes aerodynamics code, ARC2D.

Ice Accretion Simulation

A theoretical evaluation is performed to ascertain the capabilities of LEWICE, the NASA Lewis ice accretion simulation code, for large drops. Then, a parameter study is performed to show typical results

in this regime. A Twin Otter airfoil was selected for these runs, as large droplet ice shapes were generated on this model in the IRT. A range of drop sizes from 10 micron to 1000 micron was selected. These limits were chosen so as to fill out a log scale plot. Local and total collection efficiencies, impingement limits, and maximum local collection efficiency are presented.

This paper will also present the assumptions used in the droplet trajectory code in LEWICE and will evaluate their applicability for large drops. A large drop in this context applies to any drop size larger than 40 μm , the current upper limit in the FAA certification envelope. LEWICE currently uses the following assumptions:

- solid particles
- spherical particles
- drops do not breakup due to acceleration
- particles do not rotate
- particles have no lift
- particles have no moment
- drag for a stationary sphere applies
- no transient effects due to changing drag
- evaporation of the drop is negligible
- turbulence effects are neglected
- flow is incompressible
- drops do not interact with each other
- continuum flow around drop
- all drops which strike the airfoil impinge

Drop Size Study

In a previous report¹, an analysis was performed on the droplet physics in LEWICE² to estimate the potential effect of different phenomena for drops beyond the current FAA certification envelope. That analysis used a MS-317 airfoil and showed that droplet splashing was the major factor

which needed to be accounted for in any code modification. Since then, tests have been performed in the NASA Icing Research Tunnel (IRT) on a NACA23012 airfoil and a Twin Otter Airfoil. The first part of this report will repeat some of the earlier analysis using the Twin Otter airfoil. It was chosen since the large majority of ice accretions used this airfoil.

LEWICE assumes that all drops which strike the surface impinge, thus neglecting splashing and/or bouncing of drops. A recent experimental study by Mundo, Sommerfeld and Tropea⁹ using a two-component phase doppler anemometer categorized droplet-wall collisions and correlated splashing in terms of Reynolds number and Ohnesorge number ($Oh = \sqrt{We}/Re = \mu/\sqrt{\rho\sigma d}$). These numbers are based on the liquid properties and the component of the impact velocity normal to the surface. Based on the results of their experiment, splashing occurs if the factor $K = Oh * Re^{1.25}$ is greater than 57.7. A plot of this parameter for a drop size of 160 microns is shown in Fig. 1.

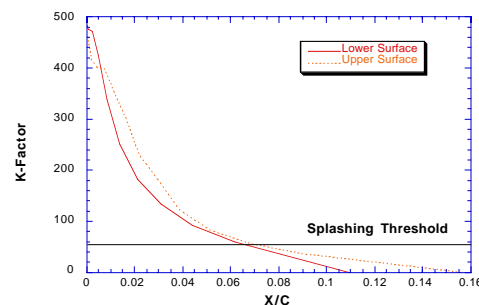


FIGURE 1. K-factor for droplet splash

A 160 micron drop size was chosen since this was the drop size used in the IRT experiment. This figure shows that, according to their research, droplet splashing is a significant factor for this drop size. The Mundo paper also provides a characterization of the size, velocity and direction of

the splashed particles. By knowing these parameters, a feature could be added to LEWICE to track the trajectories of the splashed particles and the trajectories of particles after breakup. As this modification has not yet been made, a more qualitative approach is taken by analyzing the current trends as drop size increases. This approach will now be presented.

Parameter Study

The capabilities of LEWICE in the large drop regime were evaluated by means of a parameter study on drop size. Twenty cases were evaluated using drop sizes ranging from 10 microns to 1000 microns. The airfoil used for these runs was a 6 foot chord Twin Otter airfoil. The meteorological conditions ran were:

- $\alpha = 0^\circ$
- LWC = 0.82 g/m³
- V = 195 mph
- T = 28 °F
- MVD = 10 μm to 1000 μm

Figures 2-4 show the local collection efficiency, β , of each drop size ran in this study. The maximum local collection efficiency increases with drop size, both the upper and lower limits are further downstream with increasing drop size and the total collection efficiency increases with drop size. All of these trends are expected and intuitive. Figure 2 shows a large variation over the initial drop size range while in Fig. 3 this trend slows somewhat and finally, collection efficiency is nearly the same for the very large drop size range. This occurs because the larger drops have so much inertia that their trajectory is nearly ballistic.

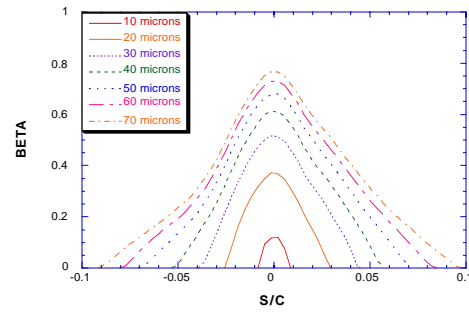


FIGURE 2. Collection efficiencies for MVD from 10 to 70

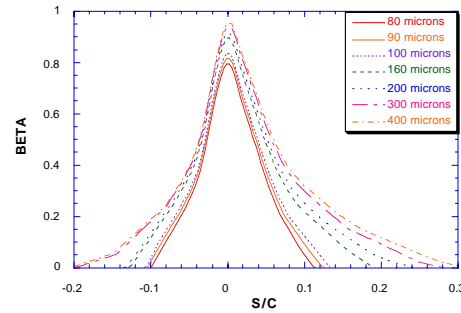


FIGURE 3. Collection efficiency for MVD from 80 to 400

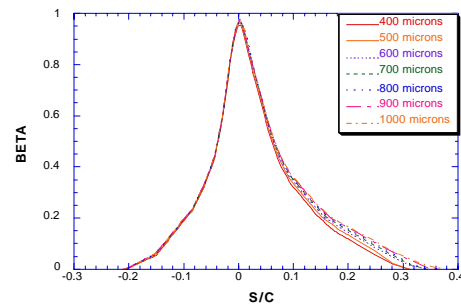


FIGURE 4. Collection efficiency for MVD from 80 to 400

Since this analysis focuses on the major characteristics, maximum collection efficiency, impingement limit and total collection efficiency, these parameters are also plotted in Figs. 5-7.

These plots reveal the reasons why there is an upper limit to the local collection effi-

ciencies shown earlier. The larger a drop gets, the more ballistic its trajectory will be and the local collection efficiency becomes simply a reflection of the curvature of the airfoil geometry.

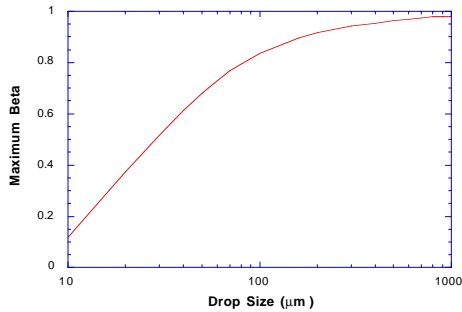


FIGURE 5. Maximum beta as a function of drop size.

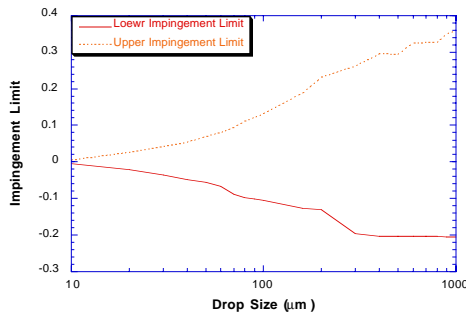


FIGURE 6. Impingement limit as a function of drop size.

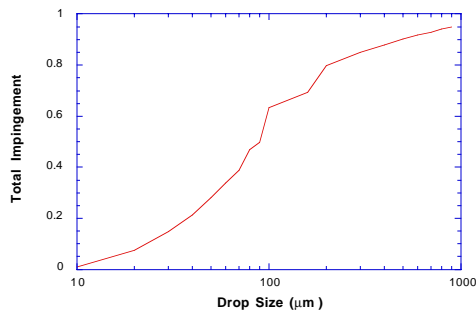


FIGURE 7. Total collection efficiency as a function of drop size.

Figure 5 shows the maximum local collection efficiency. Since this cannot, by definition, be greater than one for a Twin Otter airfoil, β_{\max} provides one limitation with drop size. Figure 6 shows the upper and lower impingement limits. The theoretical limits are the maximum and minimum thickness of the airfoil. The 1000 μm drop size impingement limit is very close to this value.

The theoretical limitations are best shown in Fig. 7. The total collection efficiency is the integral of the local values normalized to the airfoil thickness. This shows the degree to which the drops are deflected by the airfoil. If the drops come in with no deflection, the total collection efficiency is one. This curve shows a rapid increase in total collection efficiency up to 100-200 micron range, then gradually approaching a value of one at 1000 microns.

Comparison with IRT Data

In order to quantify the effect of droplet splash and other phenomena due to large drops, a comparison is made between LEWICE and experimental data taken in the IRT. The results of the IRT entry are presented in another paper at this conference.¹⁰ The first set of comparisons required no adjustments in LEWICE to account for the behavior of large drops. Discrepancies, if any, between predicted and experimental shapes are presumed to be due solely to the effects of droplet splash. Then, an empirical splashing model is created to model the case where LEWICE did not accurately predict the ice shape.

The first case, Fig. 8, is an 18 minute ice shape generated on a NACA 23012 airfoil at the following conditions: $T_0 = 28^\circ\text{F}$, $V =$

195 mph, LWC = 0.82 g/m³, MVD = 160 μm, α = 0°.

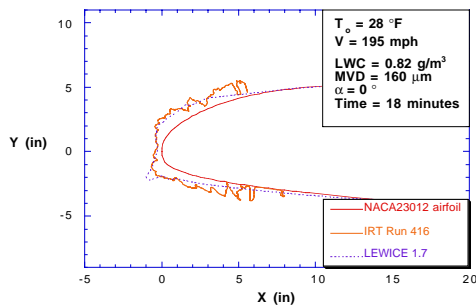


FIGURE 8. LEWICE comparison with IRT Run 416.

This is an excellent comparison for LEWICE. It should be noted that LEWICE outputs only the smooth ice shape and does not display the roughness which is predicted within the code. Due in part to the high LWC and large drop size, the predicted roughness for this case is extremely high. A maximum roughness of 2.5 mm (0.1 in) was predicted for this case, with an average roughness of 0.9 mm. It is also possible that the large feathers on the back of the IRT shape are due to droplets which splashed and reimpinged at that location.

The second case, Fig. 9, is an 18 minute ice shape generated on a Twin Otter airfoil at the same conditions as those for Fig. 8.

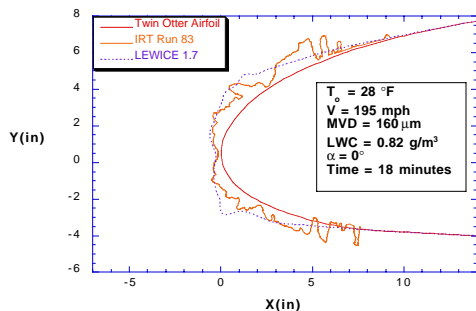


FIGURE 9. LEWICE comparison with IRT Run 83.

This case also shows excellent comparison with the IRT ice shape. Other ice shape

comparisons at warm temperatures are provided in an Appendix at the end of the report. The good comparison shown in these figures is confusing at first, since the previous analysis showed that droplet splashing is a major factor for large drop conditions and LEWICE does not account for it. A possible explanation for this discrepancy can be implied from the comparison shown in Fig. 10, which shows a comparison for a Twin Otter airfoil at a lower ambient temperature, T_o=5°F.

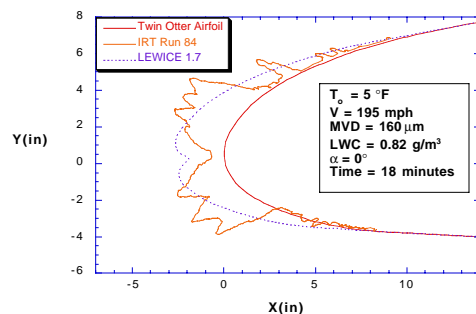


FIGURE 10. LEWICE comparison with IRT Run 84.

This comparison shows more ice in the stagnation zone and less at the horns for the predicted ice shape versus that for the IRT shape, with the overall mass being approximately the same. Normally, this would be attributed to a possible deficiency in the predicted heat transfer coefficient. However, since the predictions for warmer conditions are very good, an alternate theory will be presented which will incorporate the effects of droplet splashing.

A prediction of the change in results once droplet breakup and droplet splash are considered can now be estimated. The suggestion is that neither of these factors result in a loss of mass to the surface. The IRT ice shapes show the same amount of ice as predicted by LEWICE, even though LEWICE does not account for these effects and close up videos taken during the IRT

entry show some splashing of water. Therefore, the splashed drops may not reenter the airstream, but may actually reimpinge on the surface downstream of the initial impact location. This is illustrated in Fig. 11.

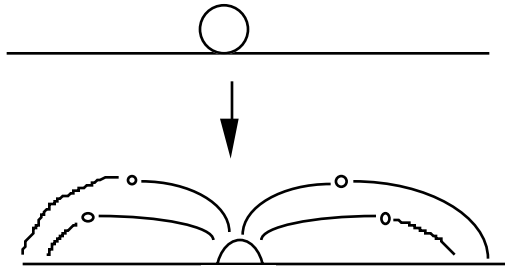


FIGURE 11. Representation of Droplet Splash

Using this model, a drop which splashes at the stagnation point will redistribute its mass to downstream regions of the airfoil. In effect, the splashed droplets behave very much like surface runback water. Thus, for high temperature conditions where much of the impinging water does not freeze, there is no difference in the ice shape generated by LEWICE, which moves the water downstream via runback, and the IRT case, which moves some of the water downstream via runback and some via splashing. For the colder temperature case however, much of the impinging water freezes and LEWICE predicts little runback. In reality, some of the water which freezes in LEWICE is splashed downstream causing more apparent ‘runback’ which was demonstrated in Fig. 10.

An empirical model is planned to account for this effect. The model will take part of the water which would have impinged and moves it to the next downstream location. The exact amount moved at each location will be computed from the K-factor described earlier.

Airfoil Performance Simulation

Simulation methods are also available for assessment of the aerodynamic impact of large droplet ice formations. These methods can be used in conjunction with wind tunnel tests to identify ice formation features that play a critical role in performance losses for a given airfoil geometry.

These calculations were performed using a 2D, Reynolds averaged, Navier-Stokes code (ARC2D)¹¹ coupled with an algebraic turbulence model¹² modified for use with ice shape geometries. The grid code used is a hyperbolic grid generator developed by Barth.¹³

Results from the current study indicate possible mechanisms for performance loss due to large droplet ice formations. This was accomplished by calculating flow solutions for airfoils with and without ice shapes on the leading edge regions. The ice shapes examined were tracings of actual ice shapes generated in the NASA Lewis Icing Research Tunnel (IRT), an artificial shape used to simulate ice for a flight test, and a LEWICE generated ice shape. The results are used to gain understanding of the aerodynamics associated with iced airfoils and to compare the aerodynamics of the real ice shape to that of an artificial ice shape.

Figures 12 and 13 show the results from a calculation of the flowfield surrounding an MS-317 airfoil with an ice shape generated in the NASA IRT. The ice shape profiles was generated for the conditions of LWC = 0.5 g/m³, a median volume diameter of 190 μm, and a total temperature of 34°F. The calculations were performed for a free stream Mach number of 0.28, a Reynolds

number of 9 million, and an angle of attack of 4 degrees.

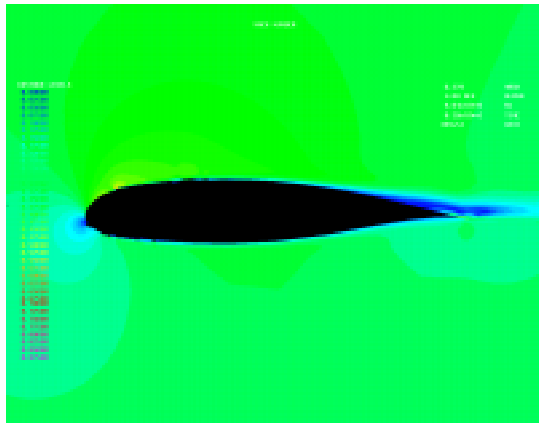


FIGURE 12. Regional transport wing section with large droplet ice accretion. $M = 0.28$, $Re = 9 \times 10^6$, $\alpha = 4$

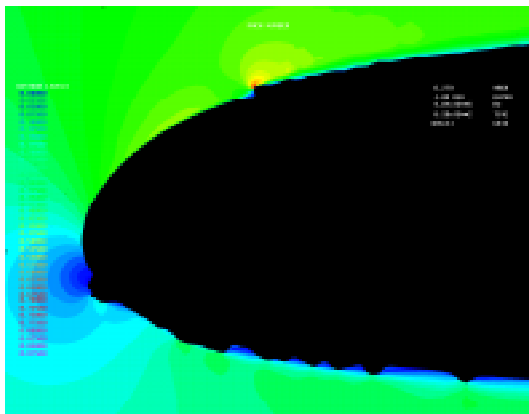


FIGURE 13. Regional transport wing section with large droplet ice accretion. $M = 0.28$, $Re = 9 \times 10^6$, $\alpha = 4$

In Fig. 12, the Mach number contour plots show a large low flow region near the trailing edge, indicated by the dark contour region. This region corresponds to a separation bubble that forms due to the momentum loss suffered by the boundary layer as it passes over the rough ice region. The roughness itself is better illustrated in Fig. 13, where the dark contour lines indicate additional regions of low flow between ice roughness elements.

The second airfoil examined was a representative regional transport wing section with a quarter round obstruction applied to the upper surface. The quarter round was 0.5 inches in height and was located at 6 percent chord.

This was done to simulate some earlier pre-flight tests performed on a runway. In those tests, the airplane wings were fitted with quarter round strips along the span of the wing and the aircraft performed a run-up to takeoff. The aircraft was actually taken to the rotation condition in order to safely determine aerodynamic performance for a wing with ice ridges aft of the protected region

Figures 14 and 15 show the Mach number contours for the regional transport both in a clean condition and with the artificial ice shape near the leading edge.

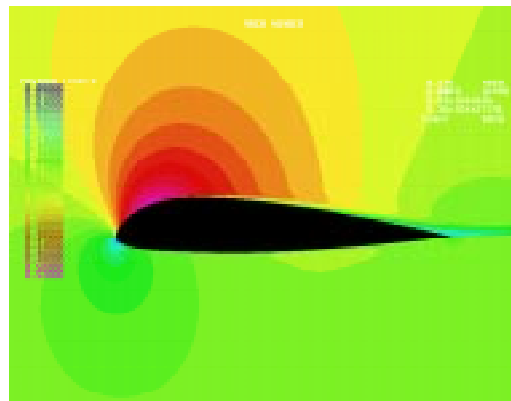


FIGURE 14. Regional transport wing section without ice accretion. $M = 0.28$, $Re = 9 \times 10^6$, $\alpha = 6$

Figure 14 shows the clean airfoil Mach number contours which indicate a normal flow pattern for an airfoil of this type. In Fig. 15, the same airfoil, except with the quarter round protuberance, displays a much different flow field. The flow is unsteady and there is considerable vortex shedding occurring aft of the airfoil. In this case, however, the shedding is not associ-

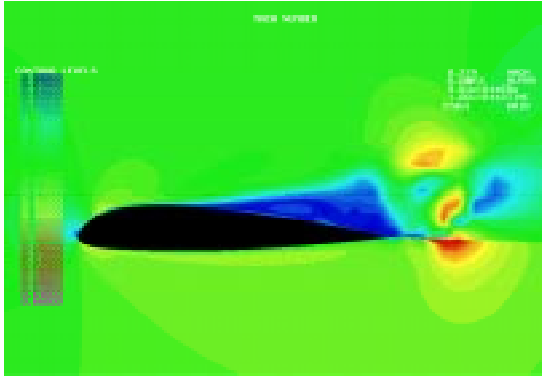


FIGURE 15. Regional transport wing section with quarter round simulated ice accretion. $M = 0.28$, $Re = 9 \times 10^6$, $\alpha = 6^\circ$ ated with a premature tail stall but is actually precipitated by the behavior just aft of the protuberance itself. This is illustrated in Fig. 16, which shows the flow field pattern in the vicinity of the artificial ice shape.

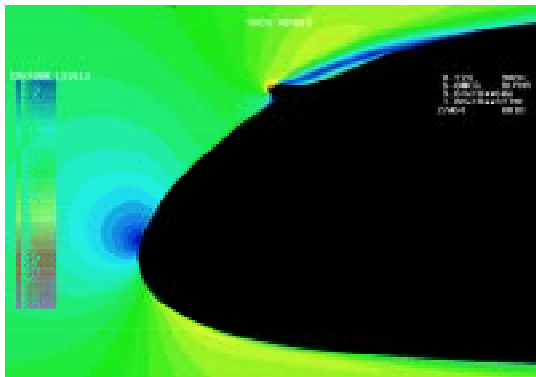


FIGURE 16. Regional transport wing section leading edge with quarter round simulated ice accretion. $M = 0.28$, $Re = 9 \times 10^6$, $\alpha = 6^\circ$

The final series of calculations were for a NACA 23012 airfoil geometry. In this case, ice shapes were obtained from a LEWICE calculation as well as from ice shape tracings obtained in the NASA IRT. The two shapes used are those from Fig. 8. The icing conditions used to generate those shapes were mentioned during the discussion of the ice shape comparisons.

Figures 17-19 show the Mach number contours calculated for those shapes and illustrate one of the difficulties in reproducing ice shapes for the purpose of aerodynamic

performance assessment, regardless of whether that assessment is experimental or computational in nature.

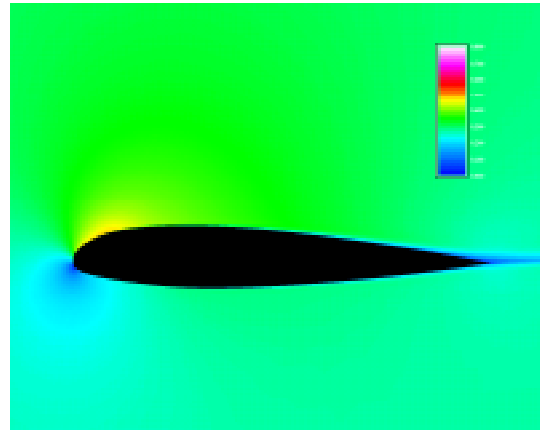


FIGURE 17. Mach No. contours for a clean NACA 23012 airfoil. $M = 0.28$, $Re = 9 \times 10^6$, $\alpha = 6^\circ$

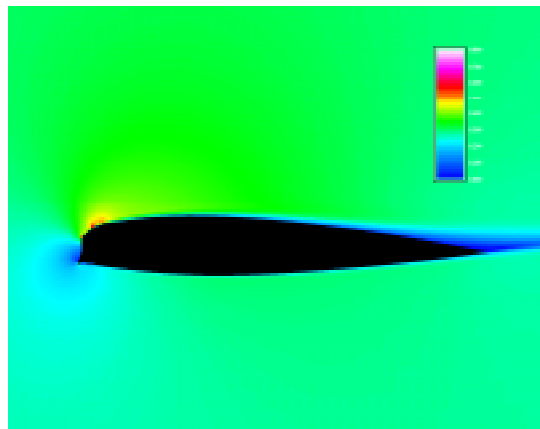


FIGURE 18. Mach No. contours for a NACA 23012 airfoil with a LEWICE generated ice shape. $M = 0.28$, $Re = 9 \times 10^6$, $\alpha = 6^\circ$

Figure 17 shows the clean airfoil results. Once again, the computation shows a well behaved flow field solution similar to results available for other airfoils of this type. In Fig. 18, the LEWICE generated ice shape has been added to the leading edge. The flow code results indicate that this ice shape has caused a premature trailing edge separation, similar to that from

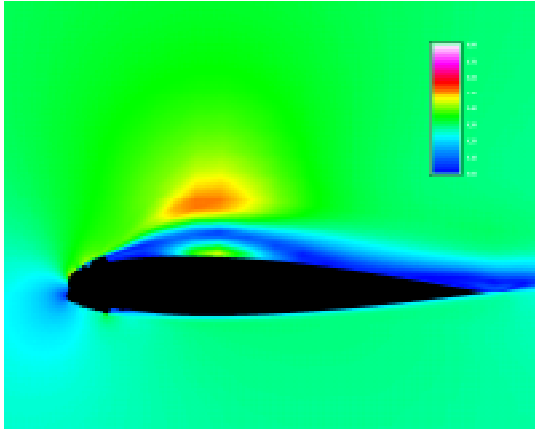


FIGURE 19. Mach No. contours for a NACA 23012 airfoil with an IRT generated ice shape. $M = 0.28$, $Re = 9 \times 10^6$, $\alpha = 6$

the MS-317 calculation, which had an IRT ice shape.

As described earlier, this LEWICE ice shape compares quite well with the ice shape obtained from the IRT under the same conditions. The ice mass, the overall thickness and the icing limits are all reproduced by the calculation. However, the flow code results for the LEWICE shape are quite different from those for the IRT ice shape, as shown in Fig. 19.

The IRT ice shape produces an unsteady leading edge stall condition with vortex shedding from the upper surface of the airfoil. Figure 19 shows only one moment in time from that shedding process. Thus, the ice shapes from LEWICE and from the IRT, although similar in shape, could produce very different performance results if tested in a dry air wind tunnel. This suggests that some additional criteria must be considered when evaluating the acceptability of ice shape simulation methods.

The desire to evaluate airfoil geometries for susceptibility to large droplet icing performance effects suggests a need for a reinvigorated code development program. A significant amount of work has been per-

formed on ice shape geometries resulting from icing conditions within the FAR-25 envelope. This work could be extended to large droplet ice shapes. It should also be tied to an aerodynamic analysis method in order to insure that the desired characteristics are included in any simulation method. If this approach is followed, it could result in a computational method for simple evaluation of large droplet icing aerodynamic impact.

Conclusions

A parameter study was performed to show the predicted collection efficiencies for large droplets and to estimate the effect of droplet splash, which is the major change which will occur in this regime. The LEWICE user is cautioned that the splashing estimates depend not only on drop size, but on velocity as well. The key parameter is the Weber number, which is proportional to drop size but is proportional to velocity squared. Therefore, velocity will play a large factor in the determination of splashing effects.

A comparison is then made with data generated in the IRT. For high temperature cases, LEWICE predicts the ice shapes extremely well. For a colder condition, LEWICE predicts more mass at stagnation and less elsewhere. It is theorized that drops which splash at stagnation reimpinge downstream.

LEWICE has been shown to be a very robust code for predicting droplet trajectories and ice accretion for numerous different conditions. Research is continuing on improving the physical models within the code in order to produce a code which can accurately predict ice shapes for any condition.

Performance evaluation using computational methods can provide an inexpensive and timely means for evaluating aircraft susceptibility to large droplet icing conditions. Results indicate that large droplet ice shapes can result in premature stall conditions and that the cause can be due to a leading edge or a trailing edge separation. The reason for stall will be dependent on the ice shape size, location, and roughness level and on the geometry of the airfoil itself.

Determination of the correct ice simulation shape to use in aerodynamic testing or analysis must include a consideration of the tremendous variation in actual ice shape profiles and roughness levels and the resulting variation in aerodynamics associated with those geometries. Some form of analytical analysis should be performed to determine the range of conditions that are to be expected from a wind tunnel test program designed to evaluate performance degradation due to large droplet ice accretions.

References

- 1) Wright, W. B., "Capabilities of LEWICE 1.6 and Comparison with Experimental Data," presented at the AHS International Icing Symposium, Montreal, Canada, Sept. 1995.
- 2) Wright, W.B., "Users Manual for the Improved NASA Lewis Ice Accretion Code LEWICE 1.6," NASA CR198355, June 1995.
- 3) Hedde T., Guffond D., "Improvement of the ONERA 3D icing code, comparison with 3D experimental shapes," AIAA 93-0169
- 4) Gent, R.W., "TRAJICE2 - A combined water droplet and ice accretion prediction code for aerofoils," Royal Aerospace Establishment TR 90054, 1990.
- 5) Brahimi, M.T., Tran, P., and Paraschi-voiu, I., "Numerical Simulation and Thermodynamic Analysis of Ice Accretion on Aircraft Wings," Centre de Développement Technologique de l'École Polytechnique de Montréal, C.D.T. Project C159, Final Report prepared for Canadair, 1994.
- 6) Potapczuk, M.G., Al-Khalil, K.M., Velazquez, M.T., "Ice Accretion and Performance Degradation Calculations with LEWICE/NS," NASA TM-105972, AIAA-93-0173, Jan. 1993.
- 7) Shin, J., Berkowitz, B., Chen, H., and Cebeci, T., "Prediction of Ice Shapes and Their Effect on Airfoil Performance," AIAA Paper 91-0264, Jan. 1991.
- 8) Kwon, O.J. and Sankar, L.N., "Numerical Study of the Effects of Icing on Finite Wing Aerodynamics," AIAA Paper 90-0757, Jan. 1990.
- 9) Mundo, C., Sommerfeld, M., and Tropea, C., "Droplet-Wall Collisions: Experimental Studies of the Deformation and Breakup Process," Int. J. Multiphase Flow, v. 21, No. 2, pp. 151-173, 1995.
- 10) Addy, G. and Miller, D., "A Study of Large Droplet Ice Accretions in the NASA-Lewis IRT at Near-Freezing Conditions; Part 2," FAA International Conference on Icing, May 1996.
- 11) Pulliam, T.H., "Euler and Thin Layer Navier-Stokes Codes: ARC2D,

ARC3D,” UTSI E02-4005-023-84,
March 1984.

12) Potapczuk, M.G., “Navier-Stokes
Analysis of Airfoils with Leading Edge
Ice Accretions,” NASA CR 191008,
February 1993.

13) Barth, T., Pulliam, T.H., and Buning,
P.G., “Navier-Stokes Computations for
Exotic Airfoils,” AIAA Paper 85-0109,
Jan. 1985.

Appendix

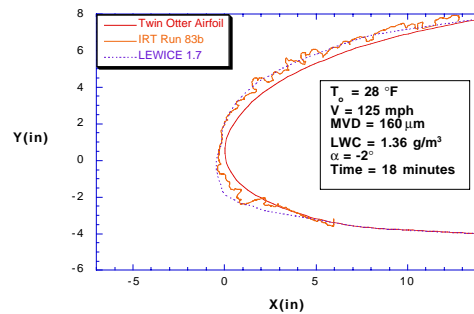


FIGURE 22. LEWICE comparison with IRT Run 83b

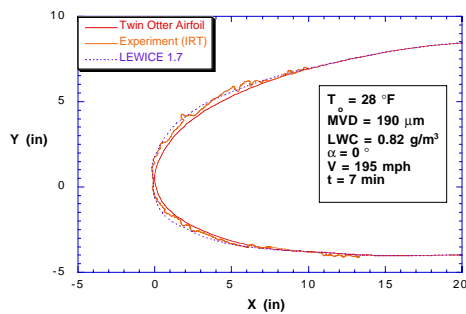


FIGURE 20. LEWICE comparison with IRT Run DC2

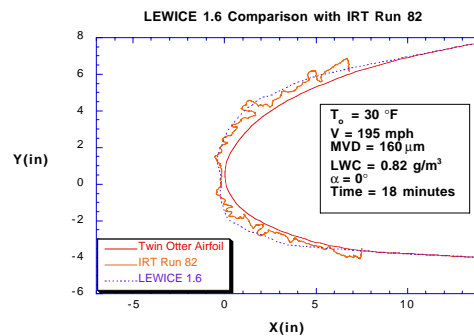


FIGURE 23. LEWICE comparison with IRT Run 82

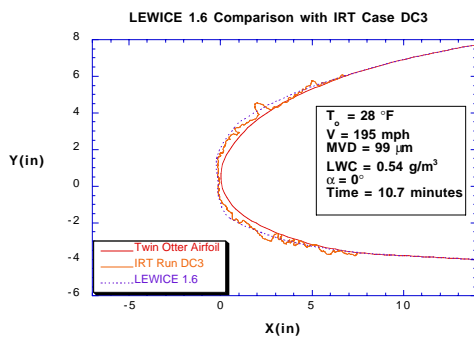


FIGURE 21. LEWICE comparison with IRT Run DC3